Convergence of models of human ventricular myocyte electrophysiology after global optimization to recapitulate clinical long QT phenotypes

Stefan A. Mann[a,b,c], Mohammad Imtiaz[a], Annika Winbo[d,e], Annika Rydberg[d], Matthew D. Perry[a,b], Jean-Philippe Couderc[f], Bronislava Polonsky[f], Scott McNitt[f], Wojciech Zareba[f], Adam P. Hill[a,b,*✉], Jamie I. Vandenberg[a,b,*✉]

a. Victor Chang Cardiac Research Institute, 405 Liverpool Street, Darlinghurst NSW 2010, Australia
b. St Vincent's Clinical School, University of New South Wales, Australia
c. Current Address: Cytocentrics Bioscience GmbH, Cologne, Germany
d. Department of Clinical Sciences, Pediatrics, Umeå University, 90185 Umeå, Sweden
e. Current address: Department of Physiology, University of Auckland, Auckland, New Zealand
a. Division of Cardiology, University of Rochester School of Medicine, Rochester, New York, USA.

Short title: Optimizing *in-silico* human ventricular AP models

*** Joint Corresponding Authors**

Jamie I. Vandenberg
Department of Molecular Cardiology and Biophysics,
Victor Chang Cardiac Research Institute, 405 Liverpool Street, Darlinghurst NSW 2010, Australia
e-mail: j.vandenberg@victorchang.edu.au
Phone +61 2 9295 8600

Adam P Hill
Department of Molecular Cardiology and Biophysics,
Victor Chang Cardiac Research Institute, 405 Liverpool Street, Darlinghurst NSW 2010, Australia
e-mail: a.hill@victorchang.edu.au
Phone +61 2 9295 8600

Abstract

In-silico models of human cardiac electrophysiology are now being considered for prediction of cardiotoxicity as part of the preclinical assessment phase of all new drugs. We ask the question whether any of the available models are actually fit for this purpose. We tested three models of the human ventricular action potential, the O'hara-Rudy (ORD11), the Grandi-Bers (GB10) and the Ten Tusscher (TT06) models. We extracted clinical QT data for LQTS1 and LQTS2 patients with nonsense mutations that would be predicted to cause 50% loss of function in I_{Ks} and I_{Kr} respectively. We also obtained clinical QT data for LQTS3 patients. We then used a global optimization approach to improve the existing *in silico* models so that they reproduced all three clinical data sets more closely. We also examined the effects of adrenergic stimulation in the different LQTS subsets. All models, in their original form, produce markedly different and unrealistic predictions of QT prolongation for LQTS1, 2 and 3. After global optimization of the maximum conductances for membrane channels, all models have similar current densities during the action potential, despite differences in kinetic properties of the channels in the different models, and more closely reproduce the prolongation of repolarization seen in all LQTS subtypes. *In-silico* models of cardiac electrophysiology have the potential to be tremendously useful in complementing traditional preclinical drug testing studies. However, our results demonstrate they should be carefully validated and optimized to clinical data before they can be used for this purpose.

Highlights:

- LQTS causes action potential prolongation by genetically heterogeneous mechanisms.
- Current *in silico* models cannot reproduce clinical data for major LQTS subtypes.
- We optimized *in silico* models to reproduce APD prolongation for LQTS1, 2 &3.
- Following optimization, models converged to have similar membrane conductance levels.
- These optimised models are better starting points for assessing drug toxicity.

Key words: Repolarization; long QT syndrome; *in-silico* models; adrenergic regulation; global optimization, computational cardiology.

Abbreviations

LQTS	long-QT syndrome
VM	ventricular myocyte
APD	Action potential duration
I_{Kr}	rapidly activating delayed rectifier current
I_{Ks}	slowly activating delayed rectifier current
I_{NaL}	late (persistent) sodium current
I_{CaL}	L-type calcium current
NCX	Sodium-calcium exchanger
NaK	Sodium-potassium pump

Introduction

Over the last 50 years, efforts to model the cardiac action potential and the electrocardiogram have evolved to the stage where they stand at the threshold of clinical application [1]. For example, the Food and Drug Administration (FDA) sponsored Comprehensive In Vitro Proarrhythmia Assay (CiPA) initiative, aimed at better pro-arrhythmic risk stratification for new drug entities, has *in-silico* modelling at its core [2]. However, while there is no doubt that computational models are invaluable tools for quantitative hypothesis testing [3], one must be cautious about using models to extrapolate to systems beyond the constraints that were used to develop the model in the first place.

Many models of the ventricular action potential have been published over the last decade (e.g. [4] [5] [6]). A more comprehensive list of models (for human, as well as other species) can be accessed from the CellML repository [7]. When considering these models, it is striking that there are considerable differences between them both in terms of the gating kinetics as well the maximal conductance of the membrane currents that contribute to repolarization. One possibility is that these different models each represent individual 'good enough' solutions that occur amongst the large population of possible solutions that can reproduce the normal action potential at baseline [8-11]. An alternative possibility is that they are optimized solutions based on partial datasets and so are sub optimal for predicting outcomes in different circumstances.

Congenital LQTS is a genetically heterogeneous condition, with at least 14 different genetic subtypes [12]. The major subtypes are LQTS1, which is caused by mutations in *KCNQ1* and results in reduced I_{Ks} current; LQTS2, which is caused by mutations in *KCNH2* and results in reduced I_{Kr} current; and LQTS3, which is caused by mutations in *SCN5a* resulting in an increased level of the late sodium current (I_{NaL}) [13]. Given that these genetically determined conditions all result in similar phenotypes, despite very different molecular bases, we reasoned that the extent of prolongation of repolarization caused by these different genetic subtypes of LQTS should provide a useful dataset with which to constrain *in silico* models of the human ventricular action potential.

In this study, we show that three contemporary models of the human ventricular action potential which we refer to as TT06 [4]; GB10 [5] and ORD11 [6] do not reproduce the clinically observed QT prolongation seen in the congenital Long QT syndromes. We then test the hypothesis that a global optimization of the expression levels of cardiac ion channels within *in-silico* models can be performed using constraints from QT data for different subtypes of LQTS. Furthermore, since subtypes of the long QT syndrome are differentially modulated by sympathetic tone [14], we use published data describing the effect of epinephrine infusion on changes in QT interval in different subtypes of LQTS to determine adrenergic control of the repolarization reserve. Following global optimization, all models tested reproduce clinical QT data more faithfully.

Methods

Clinical datasets

Data were obtained from the International LQTS registry database held at the University of Rochester Medical Centre, NY and the Centre for Cardiovascular Genetics, Umeå University, Umeå, Sweden. Four cohorts were collected. Patients with heterozygote nonsense mutations in *KCNQ1* (LQTS1 cohort), heterozygote nonsense mutations in *KCNH2* (LQTS2 cohort), heterozygote mutations in *SCN5a* (LQTS3) and the genotype-negative siblings of affected individuals in the three genetic subtypes (control cohort). We chose to focus on nonsense mutations in LQTS1 and LQTS2 as there is a large number of these mutations and even when nonsense mutations are in different locations within the transcript they should undergo nonsense-mediated decay [15] and so result in 50% reduction in channel function. We could not do this for LQTS3 as SCN5a mutations in LQTS result in a gain of function and so we have included all heterozygote mutations for this cohort.

Baseline QTc measurements were typically obtained from lead II on standard resting 12-lead electrocardiograms. Mean QT interval of at least three consecutive beats, corrected for heart rate using the RR interval preceding the beats were corrected using

Bazett's formula: QTc = QT / √RR. To minimize the confounding influence of patient specific variation in the heart rate dependence of QT intervals [16], we restricted our analysis to patients who had a resting heart rate of <70 beats per minute.

Data for the influence of epinephrine infusion on changes in QT interval in different genetic subtypes were derived from the data presented by Ackerman and colleagues [14] (see Fig. 1).

Model simulations

Simulations were carried out in Matlab 2016a. The ORD11 model was downloaded from the Rudy Lab website (http://rudylab.wustl.edu/). The TT06 model was downloaded from the CellML repository (https://www.cellml.org/) and converted into Matlab code using Cellular Open Resource [17]. E. Grandi kindly provided the GB10 model code (https://somapp.ucdavis.edu.edu/Pharamcology/bers/). All models were run in the endocardial configuration. Following a change in any parameter the model outputs will take a variable number of beats to reach a new steady-state, depending on the model as well as which parameter was changed. We determined that it took up to 450 beats for the ORD11 model to come to stead-state for any change in parameter, ~200 beats for the TT06 model and ~150 beats for the GB10 model. In our optimization routines we therefore ran each model for this corresponding number of beats before calculating the APD90 values for that parameter set.

Long QT syndrome phenotypes were modeled by reducing I_{Ks} by 50% (LQTS1), reducing I_{Kr} by 50% (LQTS2) or increasing the late sodium current I_{NaL} (LQTS3). For the TT06 and GB10 models, which do not contain a description of I_{NaL}, we introduced the I_{NaL} description from the ORD11 model. In ORD11, CaMK modulates a proportion of the fast I_{Na} as well as I_{NaL} [6]. The proportion of channels affected by this does not exceed 15%, and the modulation is of minor significance for I_{NaL} (data not shown). Because of the differences in implementation of Ca^{2+} handling between the models, when implementing I_{NaL} in the TT06 and GB10 models we did not include the modulation by CaMK

Parameter optimization

For the parameter optimization problem the objective function we were solving was a set of simulated APD_{90} outputs. As it was not possible to determine the first or second derivatives of the objective function, we were not able to use gradient search methods but instead used a pattern search algorithm. This was implemented using the "patternsearch" function in the Matlab Global Optimization Toolbox, Mathworks, Natick, MA, USA). For each of the channels, transporters and pumps chosen for our optimization process, we included simple scaling factors for the maximum conductance in the models. Specifically, we included scaling factors for I_{Kr}, I_{Ks}, I_{CaL}, I_{NaL}, I_{NaCa} and I_{NaK}. We also applied scaling factors to the degree of upregulation of I_{CaL} and I_{Ks} that occurs under increased adrenergic tone, as well as the degree of upregulation of I_{NaL} that occurs in LQTS3 (see Figure 4). We did not modify the voltage dependence of gating in any of the descriptions. For each iteration of the optimization routine, the values for these scalars were varied and the models were paced until they reached steady-state (see above). APD_{90} was determined by an automated algorithm and expressed as a % prolongation with respect to the baseline APD_{90} at 60bpm for each model. APD_{90} prolongation factors were compared to the target values compiled from the clinical data (see Fig. 1 below). The optimization minimized the sum of squares of the errors for 8 different outputs (correct baseline APD_{90}, correct adrenergic shortening in CTRL, correct baseline prolongation in LQTS1-3, and correct prolongation in LQTS1-3 under adrenergic conditions) to achieve amounts of APD_{90} prolongation that closely resembled QT prolongation in our clinical datasets (see also Fig. 4 below).

The optimization procedure employed does not allow for generation of confidence intervals for each modified scalar. We therefore investigated how sensitive the final solution, i.e. the minimized sum of squares of the errors for all 8 outputs (correct baseline APD_{90}, correct adrenergic shortening in CTRL, correct baseline prolongation in LQTS1-3, and correct prolongation in LQTS1-3 under adrenergic condition) was to small perturbations in each parameter. From this analysis, we calcuated sensitivity coefficients (ρ) for each parameter estimate as previously described [18,19] (see Table 1 below).

Population distribution

To model population distributions of action potential durations in the different cohorts each of the ionic conductances was scaled by a different random number generated from a log–normal distribution with a mean value of 1 and variance set at 0.05, as previously described [18] [19].

Results

QT prolongation in clinical cohorts of LQTS patients.

Frequency distributions of QTc values for control, LQTS1, LQTS2 and LQTS3 patients are shown in Fig. 1. The mean QTc values were 412 ± 27 ms (mean ± SD, n=196) for controls, 463 ± 31 ms (mean ± SD, n=75) for LQTS1, 480 ± 42 ms (mean ± SD, n=97) for LQTS2 and 479 ± 56 ms (mean ± SD, n=105) for LQTS3. The effects of adrenergic stimulation on the QT interval were estimated from data in Ackerman et al. [14]. Epinephrine challenge increased heart rate from a mean of ~60bpm to ~90bpm, and decreased uncorrected QT by ~1% in control patients. This corresponds to a 21% increase in QTc (see Fig. 1B). In LQTS1 patients the QT interval was increased to 130% of the control value, which corresponds to a 59% increase in QTc. In LQTS2/3 patients the uncorrected QT interval increased to 107%, which corresponds to a 31% increase in QTc (see Fig. 1B).

Figure 1 near here

Existing models do not recapitulate baseline clinical data

We next investigated whether three published *in silico* models of the human ventricular myocyte (ORD11 [6], TT06 [4] and GB10 [5]) could recapitulate the clinical LQTS data. The resulting APD_{90} values were used as surrogate markers for the QT interval [19]. All three models produce baseline action potentials with durations between ~270ms (ORD11) and ~300ms (TT06 / GB10). The three models have very different baseline

levels of I_{Ks} (much larger in TT06 compared to ORD11 or GB10, Fig 2A) and hence show very different levels of APD prolongation when I_{Ks} is reduced by 50% to mimic LQTS1. The ORD11, TT06 and GB10 models showed 2.6%, 17.2% and 0.3% prolongation of APD_{90} (Fig. 2A), compared to 12% observed clinically in LQTS1 patients with missense mutations in I_{Ks} (Fig. 1A). The differences in I_{Kr} between the three models (Fig. 2B) are not as marked as for I_{Ks}, nevertheless they still give very different levels of APD prolongation when I_{Kr} is reduced by 50%: 42% give very different levels of APD prolongation when I_{Kr} is reduced by 50%: 42% (ORD11), 7.3% (TT06) and 11.3% (GB10) prolongation of APD_{90} (see Fig. 2B) compared to 16.5% observed clinically (Fig. 1A). LQTS3 is caused by an increase in the late sodium current, I_{NaL}. Neither the GB10 or TT06 models contain a baseline I_{NaL} current. To model LQTS3 in these models, we added the baseline I_{NaL} from ORD11 and then analysed the effect of increasing this current three-fold (see Fig. 2C) to mimic LQTS3 [20]. Increasing I_{NaL} resulted in 16.4% prolongation of APD90 in the ORD11 model, 1.8% prolongation in TT06 and 37.2% prolongation in GB10 (see Fig. 2C) compared to 16.2% observed clinically (Fig. 1A). Overall, the TT06 model was the closest to the clinical data for LQTS1, the GB10 model was best for LQTS2 and the ORD11 model was best for LQTS3. However, none of the three tested models gave reasonable estimates for all three clinical data sets.

Figure 2 near here

The results so far highlight that differences in the relative levels of I_{Kr} and I_{Ks} expression profoundly impact the relative extent of APD_{90} prolongation when modeling LQTS1/2, and different levels of membrane conductance during repolarization determine how much APD_{90} prolongation is observed when I_{NaL} is increased. The ORD11, GB10 and TT06 models differ considerably in these properties, even though they do have similar baseline values for APD_{90}. This is consistent with the observation that multiple different combinations of ion channel conductances can give similar baseline values for APD_{90} [8-10]. To illustrate this point in more detail, in Fig. 3 we show that there are multiple combinations of I_{CaL} and I_{Ks} levels in the ORD11 model that give APD_{90} values

within 5% of the baseline level (yellow band in Fig. 3A). The coloured boxes within the yellow band highlight the examples shown as individual APs on the right of Fig. 3A, which all have similar APD_{90} values. When we superimpose a 50% reduction in I_{Ks} to mimic LQTS1, only a few combinations have both a reasonable baseline APD_{90} (yellow band in Fig. 3B) as well as an appropriate level of APD_{90} prolongation in the LQTS1 simulation (red band in Fig. 3B). The APs shown to the right illustrate three examples that give ~12% prolongation of APD_{90} when simulating LQTS1 but only example 2 also had an appropriate baseline APD_{90}, i.e., lies within the intersection of the red and yellow bands.

Figure 3 near here

Optimization of *in silico* models to clinical datasets

Based on the results presented in Fig. 3, we reasoned there would only be a few combinations of ion channel conductance levels that could simultaneously satisfy the criteria of maintaining normal APD_{90} levels, while reproducing LQTS1, LQTS2 and LQTS3 at resting heart rates. The markedly different responses in LQTS1, 2 & 3 patients when exposed to adrenergic stimulation (see Fig. 1) suggest there would be even fewer combinations of ion channel conductance levels that would recapitulate LQTS1, LQTS2 and LQTS3 under both resting conditions, as well as during adrenergic stimulation. To explore this hypothesis we set up a global optimization process for each model, in which the major membrane conductances were multiplied by variable scaling factors (see Materials and Methods and Fig. 4). We also introduced adrenergic sensitivity parameters for I_{Ks} and I_{CaL}. To simulate LQTS1 and LQTS2 we reduced I_{Ks} and I_{Kr} by 50%. However, as we do not know the exact level of I_{NaL} in either our control or LQTS3 cohort we allowed both, the baseline G_{NaL} scaling factor and the amount of LQTS3 related G_{NaL} increase ($S_{NaL,LQTS3}$) to vary during the optimization process. As we allowed variation of G_{CaL} and G_{NaL}, we also let the sodium calcium exchanger NCX and the sodium potassium pump NaK to vary, to avoid excessive Ca^{2+} or Na^{+} loading of the simulated cells.

Figure 4 near here

The scaling factors representing the best solutions for each of the three models are summarized in Table 1 (see below). G_{Ks} was significantly increased for the ORD11 (5.75-fold) and GB10 (25-fold) models but not for TT06, where G_{Ks} was reduced instead (0.41-fold). G_{Kr} was increased 4.28-fold in GB10 and 2.65-fold in TT06, but unchanged in ORD11. G_{CaL} was doubled in ORD11, but relatively unchanged in TT06 and GB10. The amount of up-regulation of G_{NaL} in LQTS3 was 4.5-fold in ORD11 and 4.6-fold in TT06, but only 2.5-fold in GB10. This indicates that the overall repolarization reserve in the optimized baseline GB10 model is still lower than in the optimized ORD11 and TT06 baseline models, and therefore less depolarizing current is needed to cause a given amount of action potential prolongation.

To compare current densities between models we cannot simply compare G_{max} values for each current as the different models have different kinetic formulations for each current. This can be seen by comparing the current profiles for I_{Kr}, I_{Ks}, I_{CaL} and I_{NaL} for each of the three models at baseline, after optimization and after optimization with adrenergic stimulation are shown in Figure 5A-D. To compare the current densities more directly we have calculated the integrated charge flux through each channel during the action potential. From Figure 5E, it is clear that the charge flux for I_{Kr} and I_{Ks} are much more similar in the optimized models than they are in the baseline models. For example, the charge flux for I_{Ks} ranged from 1.2 nC (GB10) to 131 nC (TT06) in the baseline models but only from 40 nC (GB10) to 105 nC (ORD11) in the optimized models. Thus, the three models appeared to converge after optimisation, at least with respect to the amount of charge flux through individual channels.

Figure 5 near here

Table 1

Summary of model scaling factors after optimization.

	ORD11		TT06		GB10	
	Scalar	ρ	Scalar	ρ	Scalar	ρ
G_{Ks}	5.75	-0.13 ± 0.01	0.41	-0.59 ± 0.06	25.02	-0.04 ± 0.05
G_{Kr}	1.00	0.66 ± 0.04	2.65	0.10 ± 0.02	4.28	0.21 ± 0.11
G_{CaL}	2.01	-0.07 ± 0.05	0.79	-0.21 ± 0.03	1.06	-0.06 ± 0.03
NCX	2.95	0.05 ± 0.02	2.08	-0.07 ± 0.08	3.69	0.00 ± 0.11
NaK	9.12	-0.09 ± 0.04	2.67	0.02 ± 0.08	4.93	0.01 ± 0.05
G_{NaL}	1.00	-0.04 ± 0.05	3.18	-0.10 ± 0.03	3.4	0.02 ± 0.10
$S_{NaL\text{-}LQT3}$	4.48	-0.17 ± 0.10	4.60	-0.04 ± 0.03	2.53	0.02 ± 0.06
$S_{Ks,Adrenergic}$	1.55	0.24 ± 0.03	2.61	0.07 ± 0.07	3.13	0.18 ± 0.16
$S_{CaL,Adrenergic}$	4.69	0.07 ± 0.10	3.08	-0.17 ± 0.05	1.78	-0.03 ± 0.17

Scalars are multipliers that alter the maximum conductance of the corresponding current component. $S_{NaL,LQTS3}$, $S_{CaL,adrenergic}$, and $S_{Ks,adrenergic}$, are applied in addition to their corresponding baseline scalar. The sensitivity coefficients (ρ) indicate how sensitive the total error function for optimized APD90 outputs for the 8 conditions are to changes in each scalar. The larger the value of ρ, the more sensitive the output is to changes in this parameter.

Whilst the individual models have converged they have still generated slightly different estimates for G_{max} (and charge flux) for each current. The algorithm we have used does not permit us to directly extract a confidence interval for each parameter estimate. To overcome this, we have employed a partial least squares analysis routine to determine sensitivity coefficients for each individual parameter. The sensitivity coefficients are summarised in Table 1. The sensitivity coefficients can be thought of qualitatively as being inverse to confidence intervals. Thus the parameters with the smallest sensitivity coefficients are the parameters that have least impact on the APD_{90} outputs and so could vary quite substantially without impacting the final result. Conversely, the parameters with large sensitivity coefficients are the ones that have most impact on the optimization results. The TT06 model is most sensitive to changes in G_{Ks},

G_{Cal} and S_{Cal_Adr}, GB10 is most sensitive to changes in G_{Kr} and S_{Ks_Adr}. Lastly, ORD11 is most sensitive to changes in G_{Kr}, G_{Ks}, S_{Ks_adr} and $S_{NaL\text{-}LQT3}$. That the different models are more sensitive to different parameters suggest that they are still quite different to each other despite the apparent convergence of overall charge fluxes.

Given that there were quite substantial changes to the optimized parameter sets for each model, we checked whether this had fundamentally altered the model response to an independent dataset, i.e. the response to changes in pacing rate. All models still showed a frequency dependent shortening of APD (see supplementary Figure 1). The extent of shortening varied more between the different models than it did between optimized and baseline versions of each model. The biggest discrepancies between the models and the experimental data occurred at the slowest pacing rates although the three optimized models were more similar to each other and more similar to the experimental data than were the original models.

The action potential waveforms, and responses to LQTS1-3, for the optimized models are shown in Fig. 6. The changes introduced by our optimization process result in more realistic APD prolongation values (albeit not perfect) for all three models. For example, LQTS1 causes 14% (ORD11), 10% (TT06) and 8% (GB10) prolongation, which are closer to the 12% observed clinically than was the case for the original models (see Fig. 2). Further, in the presence of adrenergic stimulation the LQTS1 simulations show 29% (ORD11), 29% (TT06) and 31% (GB10) APD_{90} prolongation compared to 30% QT prolongation observed clinically. The changes in APD_{90} for LQTS1-3 in control and after adrenergic stimulation are summarized in Fig. 6C where the horizontal lines represent the clinical data and the filled circles show the outputs from the optimized models at baseline and after adrenergic stimulation. We have also shown the outputs for the pre-optimized models for control and baseline LQTS1-3 in open circles, which are clearly inferior to our optimized models.

Figure 6 near here

Modeling population distribution of LQTS subtypes

To this point we have focused on single models and the mean QTc values for the different patient groups. However, there is a clearly a population distribution for QTc values within all three groups of patients (see Fig. 1). To investigate whether the optimized models were able to reproduce the clinically observed population distributions we utilized the approach originally developed by Sobie [21] for introducing random variation in the levels of expression of ion conductances in the optimized baseline models (see Fig. 7A). The frequency distribution data shown in Fig. 7 are the outputs from the optimized TT06 model with a log normal distribution of randomized scaling factors applied to all of the conductances at baseline (Fig. 7B) and when simulating LQTS1, 2 and 3 (Fig. 7C-E). The shaded distributions in Fig. 7B-E are plots of the clinical data from Fig. 1. The distributions for the modeling outputs compared to the clinical datasets are summarized as box and whisker plots in Fig. 7F. The distributions for the control, LQTS1 and LQTS2 datasets match the clinical data reasonably well, taking into account the offset between the mean of the model output for LQTS1 and the mean QTc in the LQTS1 clinical dataset. Conversely, the observed distribution for the clinical data in LQTS3 is much more variable than that seen in the model outputs. We modeled LQTS1 and LQTS2 as a 50% reduction in I_{Ks} / I_{Kr}, which should match the clinical datasets for LQTS1 and LQTS2 fairly closely as we only used data for nonsense mutations in the LQTS1 and LQTS2 cohorts. Conversely, in the model we have simulated LQTS3 using a single I_{NaL} scaling parameter, whereas in the clinical dataset there was a wide range of SCN5a mutants that would have a range of phenotypes on top of the general background of variation in the general population

Figure 7 near here

Discussion

Painstaking molecular and cellular experimental work combined with careful cellular level *in silico* model development over the last few decades has greatly improved our understanding of the quantitative basis of cardiac electrical activity [3]. However, before we can realize the full potential of this technology it is vitally important that the underlying cellular models are as good as they can be. In this study, we have developed a global optimization process utilizing independent data sets, derived from clinical LQTS cohorts, to constrain conductance parameters of *in silico* models of cardiac ventricular myocyte electrophysiology. We started with three different models (ORD11, TT06 and GB10) that had very different baseline parameters, none of which reproduced the characteristics of the clinical LQTS cohorts. After optimization, all three models give a much more realistic prolongation of repolarization for LQTS1-3 at rest as well as under increased adrenergic tone.

Whilst many *in-silico* models of cardiac electrophysiology share common components, all of them have their own unique properties. This does not surprise and illustrates the fact that in over-determined models it is expected that multiple combinations of different values for the conductance variables can give rise to similar outputs [22]. Furthermore, each of these models were optimized to reproduce data obtained from different sets of cellular experimental studies, which themselves can also be quite variable. The impact of different durations of protease digestion during cell preparation [23] [24], the influence of subtle temperature changes [25,26] and subclinical disease states on current densities [27]. These models also used different mixtures of Hodgkin Huxley and Markov state formalisms for ion channel gating kinetics. Another possibility is that each of these different models represent individual solutions that exist within the existing population where different combinations of the same components are able to perform the same biological function [10]. Nevertheless, when we applied an optimization routine relying just on altering conductance values,, we were able to generate optimised models that reproduced all the clinical data sets. Whilst all of the models were more similar after optimsation than they were at baseline in terms of charge flux densities for each current measured during the action potential (see Fig. 5) they did

not produce identical solutions. For example there was still 2-3 fold variation in charge flux for I_{Ks}, I_{CaL} and I_{NaL} in the different models (see Figure 5E). One possibility is that there are indeed multiple distinct solutions within a population of individuals that can produce similar outputs (see e.g. [28]). Another possibility is that we have not provided sufficient constraints to obtain the optimal solution. For example, we have not included optimization of calcium transient outputs [29]. To fully test this hypothesis will require a formal comparison of the "good enough solutions" concept [10],[28] versus our optimization approach using as wide a range of physiological outputs as possible.

As in all modeling studies we have made a number of assumptions that it is important to highlight so that our optimized models are used with an appropriate level of caution. First, we have only simulated single cell responses. The sheer number of independent simulations that have to be performed in a global optimization process (about $3.5x10^6$ beats in total for this study) made this approach necessary, as multicellular simulations on that scale would not have been feasible. We consequently used APD_{90} as a surrogate marker for the QT interval. Whilst this is a very reasonable assumption for single cell studies, additional factors including heterogeneity of cellular properties, as well as tissue architecture and conduction velocity, also contribute to the QT measured in an intact heart. Second, we have assumed 50% reductions of I_{Ks} in LQTS1 and I_{Kr} in LQTS2. This is based on the assumption that all mutations that result in premature termination of translation (stop codons / frameshifts with premature truncation) will result in nonsense mediated decay [30]. That such mutants undergo nonsense-mediated decay is well established. However, it is possible that where premature stop codons occur early in the protein sequence that re-initiation of translation at downstream methionines could result in expression of polypeptides that may have some function [31]. Conversely, in our LQTS3 cohort we included all *SCN5a* mutations, which presumably would include a variety of changes in the amount of I_{NaL}, rather than the single value included in our optimization process. Third, in our optimization of responses to adrenergic stimulation we only included variation in simple scaling factors for I_{Ks} and I_{CaL}. This is clearly an oversimplification with previous studies showing that adrenergic stimulation not only increases I_{Ks} and I_{CaL} current density but it also alters the voltage-dependence of I_{Ks} gating [32] and the calcium dependence of I_{CaL} inactivation [33]. Furthermore, adrenergic

stimulation causes marked changes in calcium fluxes across the SR membrane [34], which has not been included in our models. Nevertheless, the scaling factors that came out of the optimization process, between 1.55 – 3.13 for I_{Ks} up-regulation, and 1.8-4.7 for I_{CaL} up-regulation, fall into the range of what has been reported previously in *in vitro* experiments [35]. As LQTS is caused by defects in membrane conductance, we felt comfortable focusing on membrane conductances for this study. However, even in simple arrhythmia syndromes, such as LQTS, the generation of arrhythmias also involves abnormal calcium handling. Thus before these models could be used to study more complex phenomena such as the generation of early after depolarizations and arrhythmias, it would be necessary to include adrenergic effects on calcium handling and to optimize model outputs against experimentally determined calcium transients.

A surprising effect we did not anticipate was that in adrenergic simulations, especially in the TT06 model, late sodium current is reduced compared to baseline (Fig. 5D). This can be explained by the observation that the increased Ca^{2+} influx causes the action potential plateau to rise closer to the reversal potential for Na^{+} and reduce the driving force for Na^{+} influx. This observation might contribute to why LQTS3 patients generally have low risk for cardiac events when exercising, and increased risk during sleep, as discussed in [36].

In recent years there has been considerable interest in the basis of the population variability in QT intervals [10,11]. In this study, we found that introduction of small random variations in the level of membrane conductances (log-normal distribution with mean of 1 and variance of 0.05) could account for the population variability observed in the control population (Fig. 7A). Furthermore, when a 50% reduction in I_{Ks} or I_{Kr} was superimposed on the population of control simulations, not only did we see the expected increase in APD_{90} but we also saw an increase in the standard deviation of the population distribution (Fig. 7). Given that one would expect to have a lower repolarization reserve in the LQTS models it is not surprising that there is an increase in the standard deviation of the population values in the LQTS simulations. In contrast, the standard deviation in the population model for LQTS3 was not as large as that seen clinically. This, however, can be explained by the fact that in our LQTS3 cohort we considered all mutations, which would we be expected to have a much more variable influence on QT prolongation

whereas in the LQTS1 and LQTS2 cohorts we included only patients with nonsense mutations in *KCNQ1* or *KCNH2*.

The work presented here has several potential applications. First, basic LQTS research needs models that are optimized to reproduce clinical data. Further, by including random variation in other membrane conductances we can use these models to interrogate population level responses to environmental and/or genetic insults [10,11]. Second, the FDA is actively investigating the possibility of using *in-silico* methods to integrate data from high throughput ion channel screens to assess the pro-arrhythmic potential of all new drugs [37]. For this initiative it is essential that the baseline models can produce clinically relevant predictions. None, of the current generation of models can reproduce LQTS1, LQTS2 and LQTS3. Our optimization approach can contribute to improving these baseline models. It is likely however that the individual ion channel components may still need more optimization as would any drug binding models. Our optimization approach could also be used to further improve models that incorporate drug binding by comparing them to the QT data obtained for well-characterized drugs, such as the datasets recently published by the FDA [38]. As with any modeling approaches there will be further iterations as more experimental data comes to hand.

Conclusion

The existing models of cardiac electrophysiology build on decades of cardiac electrophysiology research. Nevertheless, they still do not capture some clinically important responses to changes in ion channel levels. We have devised a method that can be used to rectify this situation, and propose that existing models can be updated to capture physiological responses by constraining them to available clinical data. Using an approach such as the one suggested in this report, we believe that the modified models will be more useful both in basic research as well as in projects such as the CIPA initiative [39].

Figure legends

Fig 1. QTc intervals in LQTS cohorts. A) Frequency distribution of resting QTc intervals in (i) control (mean ± SD: 412 ± 27 ms, n=196), (ii) LQTS1 patients with truncation mutants (mean ± SD: 463 ± 31 ms, n=75), (iii) LQTS2 patients with truncation mutants (mean ± SD: 480 ± 42 ms, n=97), and (iv) LQTS3 patients (mean ± SD: 479 ± 56 ms, n=105). B) Box and whisker plots summarizing the distribution of QTc intervals for control, LQTS1, 2, 3. Data are normalized to a mean QTc of 100% for control subjects. The data shown represents the median, 25-75% and 5-95% distributions. The individual data point shown to the right of each box and whisker plot shows the mean QTc value (expressed as a percentage change relative to the mean QTc observed in control patients) following an infusion of epinephrine (calculated from data in [14]).

Fig 2. Outputs from the endocardial cell model of three models of the human ventricular action potential: ORD11 [6], TT06 [4] and GB10 [5]. The three models show comparable APD_{90} values at baseline (between ~270ms and ~300ms; black traces in each panel). However, the plateau phases differ, with a triangular shape of the ORD11 model, a more rectangular shape for the TT06 model, and an intermediate shape in the GB10 model. A) baseline (black lines) and LQTS1 (50% reduction in I_{Ks}, red lines) simulations for I_{Ks} and APs for all three models. ORD11 and GB10 have very little I_{Ks}, while TT06 has pronounced I_{Ks} current. Hence, a 50% reduction in IKs results in more AP prolongation in the TT06 model compared to the ORD11 and GB10 models. B) baseline (black lines) and LQTS2 (50% reduction in I_{Kr}, blue lines) simulations for I_{Kr} and APs for all three models. GB10 has less than half of I_{Kr} compared to ORD11 and TT06. C) baseline (black lines) and LQTS3 (3-fold increase in I_{NaL}, green lines) simulations for I_{NaL} and APs for all three models. Note that the TT06 and GB10 models do not contain an I_{NaL} current in the baseline model, so a baseline I_{NaL} was added in from the ORD11 model (see methods for details). The dashed black lines for the AP traces in panel C show the baseline AP

with no I_{NaL} component for the TT06 and GB10 models. Given the same maximum conductance levels, the three models produce I_{NaL} currents of similar amplitudes. Different levels of total repolarization reserve of the three models lead to markedly different APD responses to changes in I_{NaL} levels, i.e., while TT06 barely changes, GB10 displays a marked prolongation under LQTS3 conditions and ORD11 has an intermediate phenotype.

Fig. 3. Effects of systematic variation in I_{CaL} and I_{Ks} levels on APD output under baseline and LQTS1 conditions, in the baseline ORD11 model. A) Left-hand panel shows APD_{90} values (shaded in levels of grey according to APD_{90} values) for different combinations of I_{Ks} and I_{CaL}. The region of the left hand panel highlighted in yellow shows those combinations of I_{Ks} and I_{CaL} that give APD_{90} values within 5% of the baseline model. The blue, magenta and cyan points highlight the three examples shown on the right of the panel. B) The same combinations of I_{CaL} and I_{Ks} variation as in A), give rise to different amounts of APD_{90} prolongation, when I_{Ks} is reduced by 50% to simulate LQTS1. Highlighted in yellow are the regions that give rise to APD_{90} values within +/- 5% as in A); highlighted in red are regions that give rise to APD_{90} prolongations of around 12% in LQTS1. The three pairs of representative AP waveforms shown to the right show the same amount of prolongation in LQTS1 (CTRL: black, LQTS1: red), but have a different baseline APD_{90} (see dashed line for comparison).

Fig. 4. A schematic representation of the model optimization workflow. A) For each iteration of the process, action potentials are simulated for CTRL and LQTS conditions, for baseline without adrenergic tone at a rate of 1Hz, as well as at 1.5Hz under simulated adrenergic tone (increased G_{Ks} and G_{CaL}). For each of the simulated conditions, the APD_{90} prolongation with respect to the CTRL APD_{90} is determined ($P_{LQTS1\text{-}3}$, middle AP traces). The same step is repeated with adrenergic tone ($P_{LQTS1\text{-}3,\ adrenergic}$, right AP traces). Also, in order to prevent changes of the CTRL action potential duration, its APD_{90} is compared to the original, unmodified APD_{90} of the model (P_{CTRL}, left AP traces). The sum of the prolongation factors is the objective value that our algorithm minimizes. B)

The optimization routine adjusts the baseline scaling factors "S" for the listed conductances, the adrenergic scaling factors $S_{Ks,adrenergic}$ and $S_{CaL,adrenergic}$, as well as the LQTS3 multiplier $S_{NaL,LQTS3}$, which determines how much G_{NaL} increases during LQTS3.

Fig. 5. Comparison of the major model currents before and after optimization. A) Baseline I_{Ks} amplitudes after optimization (black lines) were larger compared to the original amplitudes (grey lines) in ORD11 and GB10, but smaller in TT06. Adrenergic stimulation (orange) led to marked increases in I_{Ks} across all models. B) The ORD11 I_{Kr} component was unchanged, but TT06 and GB10 I_{Kr} were higher after the optimization. C) I_{CaL} plateau levels were higher in ORD11 and GB10 after optimization, but smaller in TT06. Adrenergic stimulation (orange) led to marked increases in I_{CaL} in ORD11 and TT06 but in GB10, I_{CaL} was only slightly affected by simulated adrenergic stimulation. D) Only the ORD11 model had an I_{NaL} component in the original formulation. After optimization, this current was slightly increased. The current was transferred into the TT06 and GB10 models. After optimization, the GB10 I_{NaL} levels were very similar to ORD11, but in TT06 the current was ~3-fold bigger. E. The integrated current density for I_{Ks}, I_{Kr}, I_{CaL} and I_{NaL} for the three original models (grey bars) and the three optimised models (black bars). In the optimised models the current densities for I_{Ks} and I_{Kr} are much more similar to each other than they are in the original models. The changes in current density between the original and optimised models are not as marked for I_{CaL}.

Fig. 6. Action potential waveforms after model optimization. A) AP waveforms for control (black), LQTS1 (red), LQTS2 (blue) and LQTS3 (green) for the three optimized models. All models show a comparable prolongation for LQTS2 and LQTS3, and a smaller LQTS1 related prolongation. Arrows show the clinically determined levels of QT prolongation that were used as target values. B) AP waveforms of models with adrenergic up-regulation of I_{Ks} and I_{CaL}. The prolongation under LQTS1 conditions is the most pronounced in all models after adrenergic stimulation. Arrows again mark the clinically determined prolongation values. C) A summary of the changes in APD_{90} prolongation in

baseline vs. adrenergic shows the same patterns for all three models after the optimization process. The horizontal solid lines show the mean resting QTc values and the dashed horizontal lines show the mean adrenergic QTc values for the clinical data sets. The open circles show the extent of APD90 prolongation in the pre-optimised models and the filled circles show the APD90 prolongation in LQTS1,2,3 under both baseline and adrenergic conditions.

Fig. 7. Simulation of population distribution of QTc values. A) Simulation pipeline for generation of families of action potentials using the optimized TT06 model as baseline. Ionic conductances in the baseline model are modified using a log–normal distribution of randomised scaling factors and this process is repeated 100 times to generate 100 different APs. The distribution of APD_{90} values for the 100 APs in B) control, C) LQTS1, D) LQTS2 and E) LQTS3 models shown as a frequency distribution. The solid line shows the best fit Gaussian distribution for the simulated distributions. The shadow shown in grey, red, blue and green show the distributions of the clinical data (taken from Fig. 1). F) A summary of the distributions (shown as box and whisker plots) for the model outputs (open boxes) and the clinical data (closed boxes). Note that the distributions show good similarity between the models and clinical data with the exception of LQTS3 where there is a much larger distribution in the clinical data than that seen in the model outputs.

Disclosures: J.I.V. and A.P.H. are members of the Ion Channel Working Group (ICWG) Rapid Response Team, which forms part of the "Comprehensive in vitro pro-arrhythmia assay" (CiPA) initiative sponsored by the Safety Pharmacology Society and the Food and Drug Administration. A.P.H. has received funding from the Safety Pharmacology Society to undertake drug assays for the ICWG.

Acknowledgements

We thank E. Grandi for sharing her original model source code for the GB10 model.

Funding sources: This work was supported by the National Health and Medical Research Council (NHMRC) of Australia, and the Australian Research Council (ARC). S.A.M. was supported by project grant APP1047506 from the NHMRC and A.P.H. supported by a Future Fellowship from the ARC. J.I.V. is supported by an NHMRC Senior Research Fellowship.

References

[1] G.R. Mirams, M.R. Davies, Y. Cui, P. Kohl, D. Noble, Application of cardiac electrophysiology simulations to pro-arrhythmic safety testing, Br J Pharmacol. 167 (2012) 932–945. doi:10.1111/j.1476-5381.2012.02020.x.

[2] P.T. Sager, G.A. Gintant, J.R. Turner, S.D. Pettit, N. Stockbridge, Rechanneling the cardiac proarrhythmia safetyparadigm: A meeting report from the Cardiac SafetyResearch Consortium, Am Heart J. (2014) 1–9. doi:10.1016/j.ahj.2013.11.004.

[3] D. Noble, Successes and failures in modeling heart cell electrophysiology, Heart Rhythm. 8 (2011) 1798–1803. doi:10.1016/j.hrthm.2011.06.014.

[4] K.H.W.J. ten Tusscher, A.V. Panfilov, Alternans and spiral breakup in a human ventricular tissue model, AJP: Heart and Circulatory Physiology. 291 (2006) H1088–100. doi:10.1152/ajpheart.00109.2006.

[5] E. Grandi, F.S. Pasqualini, D.M. Bers, A novel computational model of the human ventricular action potential and Ca transient, J Mol Cell Cardiol. 48 (2010) 112–121. doi:10.1016/j.yjmcc.2009.09.019.

[6] T. O'hara, L. Virág, A. Varró, Y. Rudy, Simulation of the Undiseased Human Cardiac Ventricular Action Potential: Model Formulation and Experimental Validation, PLoS Comput Biol. 7 (2011) e1002061–29. doi:10.1371/journal.pcbi.1002061.

[7] C.M. Lloyd, J.R. Lawson, P.J. Hunter, P.F. Nielsen, The CellML Model Repository, Bioinformatics. 24 (2008) 2122–2123. doi:10.1093/bioinformatics/btn390.

[8] A.X. Sarkar, E.A. Sobie, Regression Analysis for Constraining Free Parameters in Electrophysiological Models of Cardiac Cells, PLoS Comput Biol. 6 (2010) e1000914–11. doi:10.1371/journal.pcbi.1000914.

[9] A.X. Sarkar, D.J. Christini, E.A. Sobie, Exploiting mathematical models to illuminate electrophysiological variability between individuals, J Physiol (Lond). 590 (2012) 2555–2567. doi:10.1113/jphysiol.2011.223313.

[10] J.N. Weiss, A. Karma, W.R. MacLellan, M. Deng, C.D. Rau, C.M. Rees, et al.,

"Good enough solutions" and the genetics of complex diseases, Circ Res. 111 (2012) 493–504. doi:10.1161/CIRCRESAHA.112.269084.

[11] O.J. Britton, A. Bueno-Orovio, K. Van Ammel, H.R. Lu, R. Towart, D.J. Gallacher, et al., Experimentally calibrated population of models predicts and explains intersubject variability in cardiac cellular electrophysiology, Proc Natl Acad Sci USA. 110 (2013) E2098–E2105. doi:10.1073/pnas.1304382110.

[12] A.S. Amin, Y.M. Pinto, A.A.M. Wilde, Long QT syndrome: beyond the causal mutation, J Physiol (Lond). 591 (2013) 4125–4139. doi:10.1113/jphysiol.2013.254920.

[13] M.T. Keating, M.C. Sanguinetti, Molecular and cellular mechanisms of cardiac arrhythmias, Cell. 104 (2001) 569–580.

[14] M.J. Ackerman, A. Khositseth, D.J. Tester, J.B. Hejlik, W.-K. SHEN, C.-B.J. Porter, Epinephrine-induced QT interval prolongation: a gene-specific paradoxical response in congenital long QT syndrome, Mayo Clin Proc. 77 (2002) 413–421. doi:10.4065/77.5.413.

[15] Q. Gong, L. Zhang, G.M. Vincent, B.D. Horne, Z. Zhou, Nonsense Mutations in hERG Cause a Decrease in Mutant mRNA Transcripts by Nonsense-Mediated mRNA Decay in Human Long-QT Syndrome, Circulation. 116 (2007) 17–24. doi:10.1161/CIRCULATIONAHA.107.708818.

[16] M. Malik, K. Hnatkova, T. Novotny, G. Schmidt, Subject-specific profiles of QT/RR hysteresis, AJP: Heart and Circulatory Physiology. 295 (2008) H2356–63. doi:10.1152/ajpheart.00625.2008.

[17] A. Garny, P. Kohl, D. Noble, Cellular Open Resource (COR): A Public CellML Based Environment for Modeling Biological Function, International Journal of Bifurcation and Chaos. 13 (2004) 3579–3590.

[18] A. Sadrieh, S.A. Mann, R.N. Subbiah, L. Domanski, J.A. Taylor, J.I. Vandenberg, et al., Quantifying the origins of population variability in cardiac electrical activity through sensitivity analysis of the electrocardiogram, J Physiol (Lond). 591 (2013) 4207–4222. doi:10.1113/jphysiol.2013.251710.

[19] A. Sadrieh, L. Domanski, J. Pitt-Francis, S.A. Mann, E.C. Hodkinson, C.A. Ng, et al., Multiscale cardiac modelling reveals the origins of notched T waves in

long QT syndrome type 2, Nat Commun. 5 (2014) 5069. doi:10.1038/ncomms6069.

[20] P.B. Bennett, K. Yazawa, N. Makita, A.L. George, Molecular mechanism for an inherited cardiac arrhythmia, Nature. 376 (1995) 683–685. doi:10.1038/376683a0.

[21] E.A. Sobie, Parameter sensitivity analysis in electrophysiological models using multivariable regression, Biophys J. 96 (2009) 1264–1274. doi:10.1016/j.bpj.2008.10.056.

[22] W. Groenendaal, F.A. Ortega, A.R. Kherlopian, A.C. Zygmunt, T. Krogh-Madsen, D.J. Christini, Cell-Specific Cardiac Electrophysiology Models, PLoS Comput Biol. 11 (2015) e1004242–22. doi:10.1371/journal.pcbi.1004242.

[23] G.R. Li, J. Feng, L. Yue, M. Carrier, S. Nattel, Evidence for Two Components of Delayed Rectifier K+ Current in Human Ventricular Myocytes, Circ Res. 78 (1996) 689–696. doi:10.1161/01.RES.78.4.689.

[24] L. Virág, N. Iost, M. Opincariu, J. Szolnoky, J. Szécsi, G. Bogáts, et al., The slow component of the delayed rectifier potassium current in undiseased human ventricular myocytes, Cardiovasc Res. 49 (2001) 790–797.

[25] T. Kiyosue, M. Arita, H. Muramatsu, A.J. Spindler, D. Noble, Ionic mechanisms of action potential prolongation at low temperature in guinea-pig ventricular myocytes, J Physiol (Lond). 468 (1993) 85–106.

[26] J.I. Vandenberg, A. Varghese, Y. Lu, J.A. Bursill, M.P. Mahaut-Smith, C.L.-H. Huang, Temperature dependence of human ether-a-go-go-related gene K+ currents, AJP: Cell Physiology. 291 (2006) C165–75. doi:10.1152/ajpcell.00596.2005.

[27] T. Aiba, G.F. Tomaselli, Electrical remodeling in the failing heart, Curr Opin Cardiol. 25 (2010) 29–36. doi:10.1097/HCO.0b013e328333d3d6.

[28] C. Sánchez, A. Bueno-Orovio, E. Wettwer, S. Loose, J. Simon, U. Ravens, et al., Inter-Subject Variability in Human Atrial Action Potential in Sinus Rhythm versus Chronic Atrial Fibrillation, PLoS ONE. 9 (2014) e105897–14. doi:10.1371/journal.pone.0105897.

[29] M. Cummins Lancaster, E.A. Sobie, Improved prediction of drug-induced

Torsades de Pointes through simulations of dynamics and machine learning algorithms, Clin Pharmacol Ther. (2016) n/a–n/a. doi:10.1002/cpt.367.

[30] Q. Gong, M.R. Stump, Z. Zhou, Position of premature termination codons determines susceptibility of hERG mutations to nonsense-mediated mRNA decay in long QT syndrome, Gene. 539 (2014) 190–197. doi:10.1016/j.gene.2014.02.012.

[31] M.R. Stump, Q. Gong, J.D. Packer, Z. Zhou, Early LQT2 nonsense mutation generates N-terminally truncated hERG channels with altered gating properties by the reinitiation of translation, J Mol Cell Cardiol. (2012) 1–9. doi:10.1016/j.yjmcc.2012.08.021.

[32] C. Terrenoire, C.E. Clancy, J.W. Cormier, K.J. Sampson, R.S. Kass, Autonomic control of cardiac action potentials: role of potassium channel kinetics in response to sympathetic stimulation, Circ Res. 96 (2005) e25–34. doi:10.1161/01.RES.0000160555.58046.9a.

[33] I. Findlay, ß-Adrenergic stimulation modulates Ca2+- and voltage-dependent inactivation of L-type Ca2+ channel currents in guinea-pig ventricular myocytes, J Physiol (Lond). 541 (2002) 741–751. doi:10.1113/jphysiol.2002.019737.

[34] D. Eisner, E. Bode, L. Venetucci, A. Trafford, Calcium flux balance in the heart, J Mol Cell Cardiol. 58 (2013) 110–117. doi:10.1016/j.yjmcc.2012.11.017.

[35] G.X. Liu, B.-R. Choi, O. Ziv, W. Li, E. de Lange, Z. Qu, et al., Differential Conditions for Early Afterdepolarizations and Triggered Activity in Cardiomyocytes Derived from Transgenic LQT1 and LQT2 rabbits, J Physiol (Lond). (2011) no–no. doi:10.1113/jphysiol.2011.218164.

[36] P.J. Schwartz, S.G. Priori, C. Spazzolini, A.J. Moss, G.M. Vincent, C. Napolitano, et al., Genotype-phenotype correlation in the long-QT syndrome: gene-specific triggers for life-threatening arrhythmias, Circulation. 103 (2001) 89–95.

[37] I. cavero, H. Holzgrefe, Comprehensive in vitro Proarrhythmia Assay, a novel in vitro/in silico paradigm to detect ventricular proarrhythmic liability: a visionary 21st century initiative, (2014) 1–15. doi:10.1517/14740338.2014.915311.

[38] J. Vicente, L. Johannesen, J.W. Mason, W.J. Crumb, E. Pueyo, N. Stockbridge,

et al., Comprehensive T wave Morphology Assessment in a Randomized Clinical Study of Dofetilide, Quinidine, Ranolazine, and Verapamil, Journal of the American Heart Association. 4 (2015) e001615–e001615. doi:10.1161/JAHA.114.001615.

[39] B. Fermini, J.C. Hancox, N. Abi-Gerges, M. Bridgland-Taylor, K.W. Chaudhary, T. Colatsky, et al., A New Perspective in the Field of Cardiac Safety Testing through the Comprehensive In Vitro Proarrhythmia Assay Paradigm, Journal of Biomolecular Screening. 21 (2015) 1–11. doi:10.1177/1087057115594589.

Table 1

Summary of model scaling factors after optimization.

	ORD11		TT06		GB10	
	Scalar	ρ	Scalar	ρ	Scalar	ρ
G_{Ks}	5.75	-0.13 ± 0.01	0.41	-0.59 ± 0.06	25.02	-0.04 ± 0.05
G_{Kr}	1.00	0.66 ± 0.04	2.65	0.10 ± 0.02	4.28	0.21 ± 0.11
G_{CaL}	2.01	-0.07 ± 0.05	0.79	-0.21 ± 0.03	1.06	-0.06 ± 0.03
NCX	2.95	0.05 ± 0.02	2.08	-0.07 ± 0.08	3.69	0.00 ± 0.11
NaK	9.12	-0.09 ± 0.04	2.67	0.02 ± 0.08	4.93	0.01 ± 0.05
G_{NaL}	1.00	-0.04 ± 0.05	3.18	-0.10 ± 0.03	3.4	0.02 ± 0.10
$S_{NaL\text{-}LQT3}$	4.48	-0.17 ± 0.10	4.60	-0.04 ± 0.03	2.53	0.02 ± 0.06
$S_{Ks,Adrenergic}$	1.55	0.24 ± 0.03	2.61	0.07 ± 0.07	3.13	0.18 ± 0.16
$S_{CaL,Adrenergic}$	4.69	0.07 ± 0.10	3.08	-0.17 ± 0.05	1.78	-0.03 ± 0.17

Scalars are multipliers that alter the maximum conductance of the corresponding current component. $S_{NaL,LQTS3}$, $S_{CaL,adrenergic}$, and $S_{Ks,adrenergic}$, are applied in addition to their corresponding baseline scalar. The sensitivity coefficients (ρ) indicate how sensitive the total error function for optimized APD90 outputs for the 8 conditions are to changes in each scalar. The larger the value of ρ, the more sensitive the output is to changes in this parameter.

Figure 1

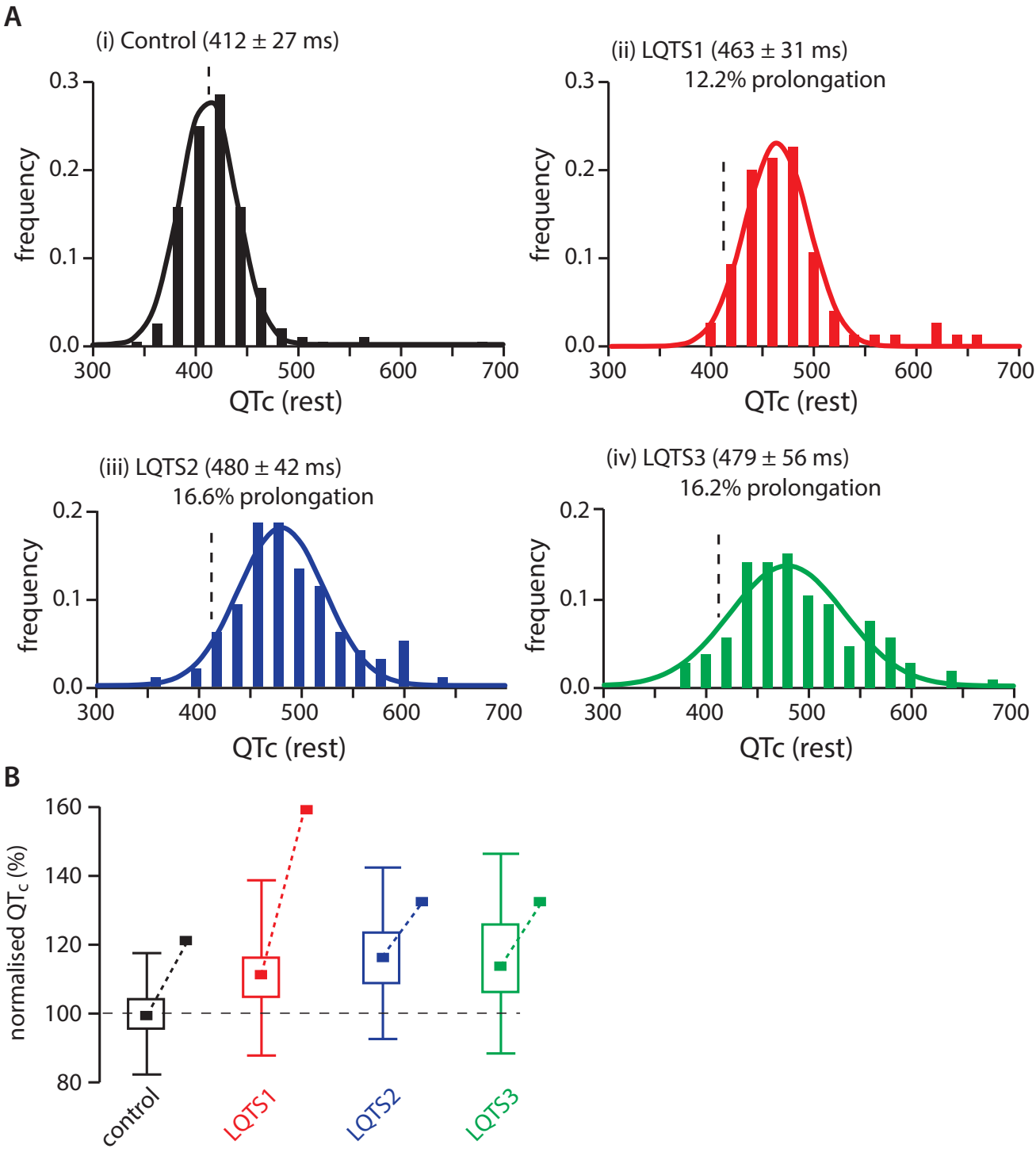

Fig 1. QTc intervals in LQTS cohorts.
A) Frequency distribution of resting QTc intervals in (i) control (mean ± SD: 412 ± 27 ms, n=196), (ii) LQTS1 patients with truncation mutants (mean ± SD: 463 ± 31 ms, n=75), (iii) LQTS2 patients with truncation mutants (mean ± SD: 480 ± 42 ms, n=97), and (iv) LQTS3 patients (mean ± SD: 479 ± 56 ms, n=105). B) Box and whisker plots summarizing the distribution of QTc intervals for control, LQTS1, 2, 3. Data are normalized to a mean QTc of 100% for control subjects. The data shown represents the median, 25-75% and 5-95% distributions. The individual data point shown to the right of each box and whisker plot shows the mean QTc value (expressed as a percentage change relative to the mean QTc observed in control patients) following an infusion of epinephrine (calculated from data in [15]).

Figure 2

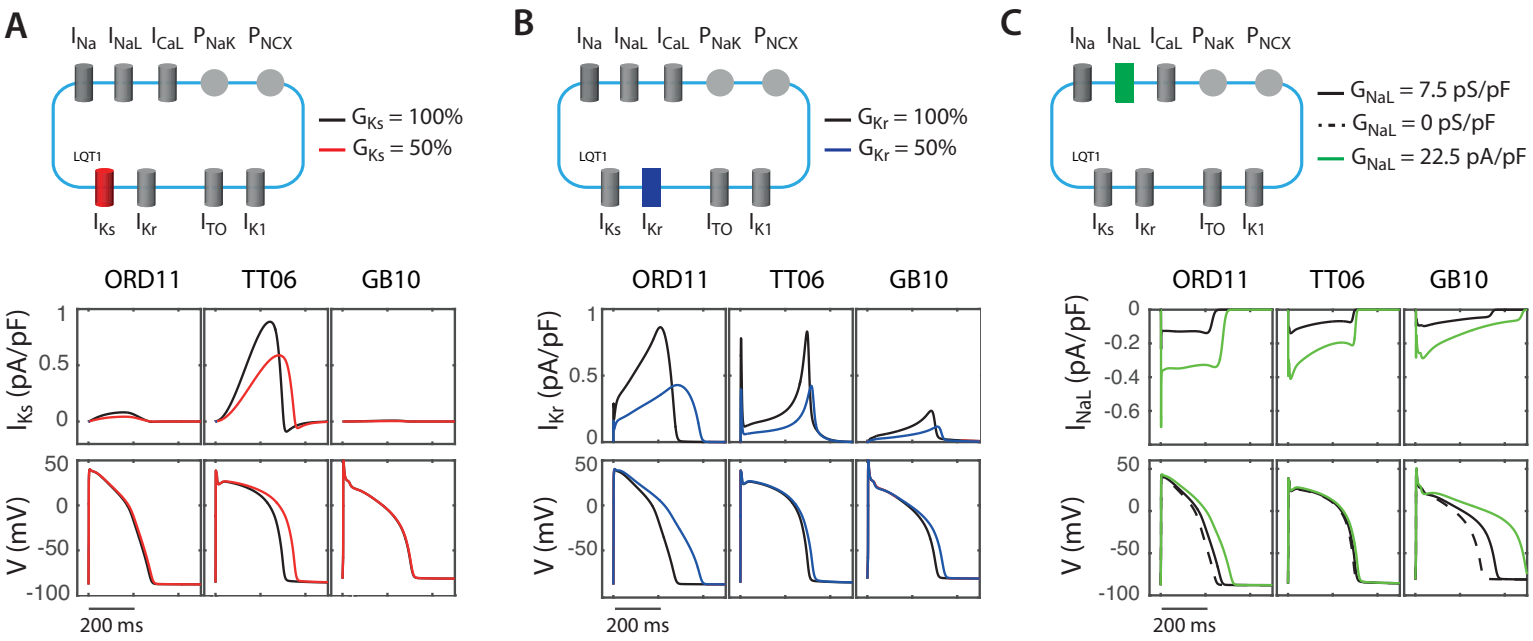

Fig 2. Outputs from the endocardial cell model of three models of the human ventricular action potential: ORD11 [6], TT06 [4] and GB10 [5].

The three models show comparable APD90 values at baseline (between ~270ms and ~300ms; black traces in each panel). However, the plateau phases differ, with a triangular shape of the ORD11 model, a more rectangular shape for the TT06 model, and an intermediate shape in the GB10 model. A) baseline (black lines) and LQTS1 (50% reduction in IKs, red lines) simulations for IKs and APs for all three models. ORD11 and GB10 have very little IKs, while TT06 has pronounced IKs current. Hence, a 50% reduction in IKs results in more AP prolongation in the TT06 model compared to the ORD11 and GB10 models. B) baseline (black lines) and LQTS2 (50% reduction in IKr, blue lines) simulations for IKr and APs for all three models. GB10 has less than half of IKr compared to ORD11 and TT06. C) baseline (black lines) and LQTS3 (3-fold increase in INaL, green lines) simulations for INaL and APs for all three models. Note that the TT06 and GB10 models do not contain an INaL current in the baseline model, so a baseline INaL was added in from the ORD11 model (see methods for details). The dashed black lines for the AP traces in panel C show the baseline AP with no INaL component for the TT06 and GB10 models. Given the same maximum conductance levels, the three models produce INaL currents of similar amplitudes. Different levels of total repolarization reserve of the three models lead to markedly different APD responses to changes in INaL levels, i.e., while TT06 barely changes, GB10 displays a marked prolongation under LQTS3 conditions and ORD11 has an intermediate phenotype.

Figure 3

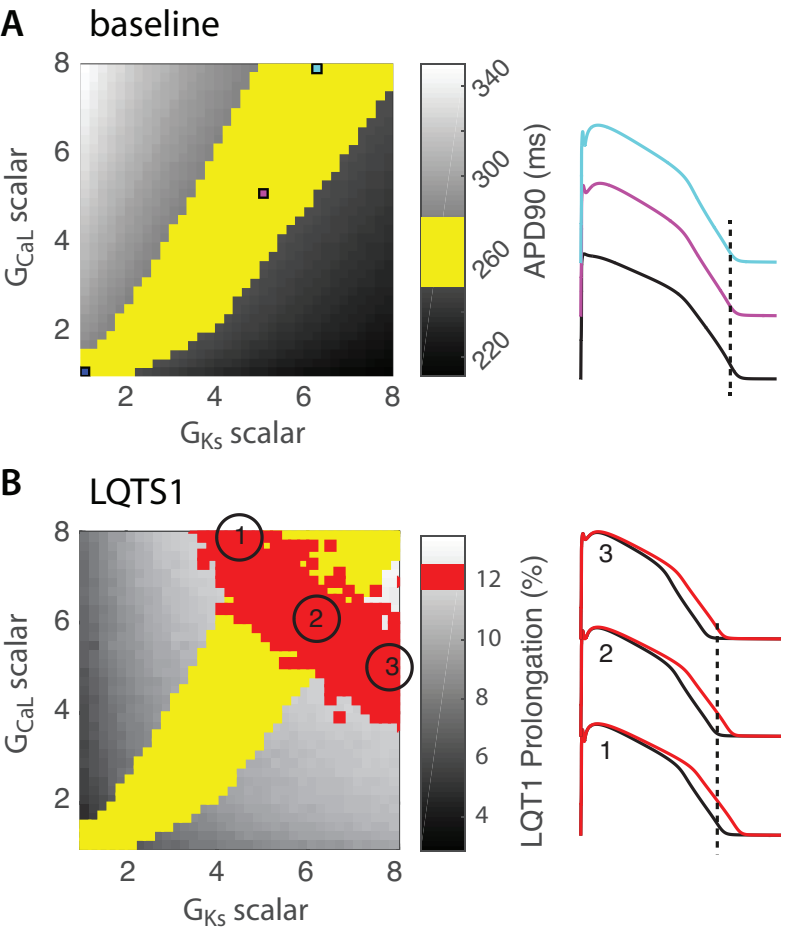

Fig. 3. Effects of systematic variation in ICaL and IKs levels on APD output under baseline and LQTS1 conditions, in the baseline ORD11 model. A) Left-hand panel shows APD90 values (shaded in levels of grey according to APD90 values) for different combinations of IKs and ICaL. The region of the left hand panel highlighted in yellow shows those combinations of IKs and ICaL that give APD90 values within 5% of the baseline model. The blue, magenta and cyan points highlight the three examples shown on the right of the panel. B) The same combinations of ICaL and IKs variation as in A), give rise to different amounts of APD90 prolongation, when IKs is reduced by 50% to simulate LQTS1. Highlighted in yellow are the regions that give rise to APD90 values within +/- 5% as in A); highlighted in red are regions that give rise to APD90 prolongations of around 12% in LQTS1. The three pairs of representative AP waveforms shown to the right show the same amount of prolongation in LQTS1 (CTRL: black, LQTS1: red), but have a different baseline APD90 (see dashed line for comparison).

Figure 4

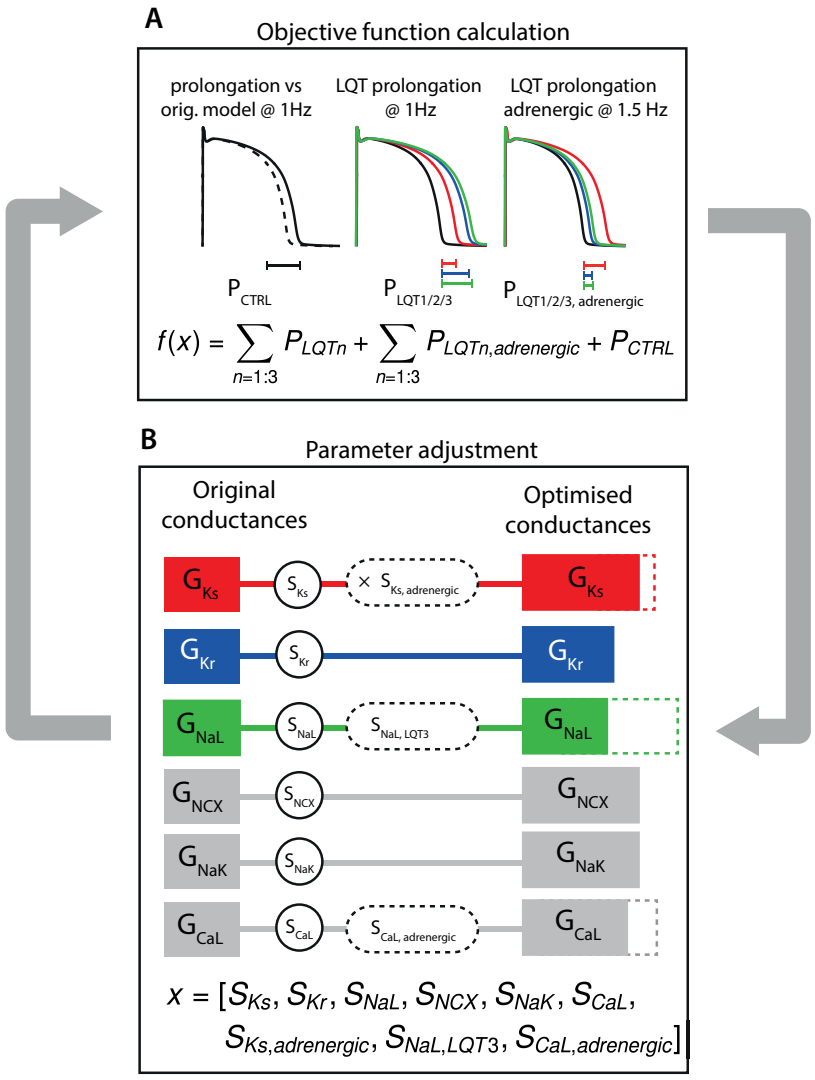

Fig. 4. A schematic representation of the model optimization workflow.
A) For each iteration of the process, action potentials are simulated for CTRL and LQTS conditions, for baseline without adrenergic tone at a rate of 1Hz, as well as at 1.5Hz under simulated adrenergic tone (increased GKs and GCaL). For each of the simulated conditions, the APD90 prolongation with respect to the CTRL APD90 is determined (PLQTS1-3, middle AP traces). The same step is repeated with adrenergic tone (PLQTS1-3, adrenergic, right AP traces). Also, in order to prevent changes of the CTRL action potential duration, its APD90 is compared to the original, unmodified APD90 of the model (PCTRL, left AP traces). The sum of the prolongation factors is the objective value that our algorithm minimizes. B) The optimization routine adjusts the baseline scaling factors "S" for the listed conductances, the adrenergic scaling factors SKs,adrenergic and SCaL,adrenergic, as well as the LQTS3 multiplier SNaL,LQTS3, which determines how much GNaL increases during LQTS3.

Figure 5

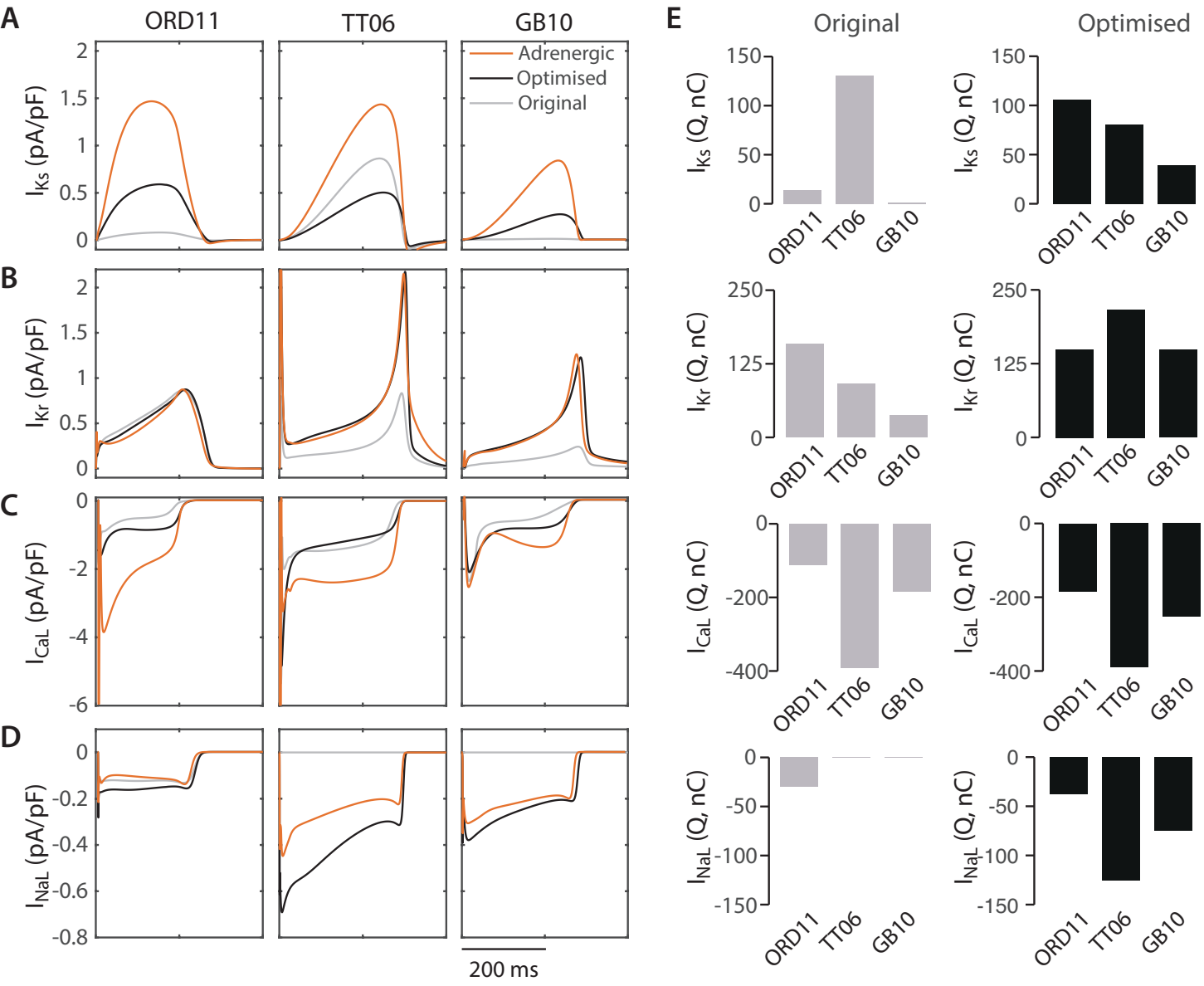

Fig. 5. Comparison of the major model currents before and after optimization.
A. Baseline I_{Ks} amplitudes after optimization (black lines) were larger compared to the original amplitudes (grey lines) in ORD11 and GB10, but smaller in TT06. Adrenergic stimulation (orange) led to marked increases in I_{Ks} across all models. The integrated current density for I_{Ks} in the original **B**. The ORD11 I_{Kr} component was unchanged, but TT06 and GB10 I_{Kr} were higher after the optimization. **C**. I_{CaL} plateau levels were higher in ORD11 and GB10 after optimization, but smaller in TT06. Adrenergic stimulation (orange) led to increases in I_{CaL} in all three models, although it was less marked in the GB10 model. **D**. Only the ORD11 model had an I_{NaL} component in the original formulation. After optimization, this current was slightly increased. The current was transferred into the TT06 and GB10 models. After optimization, the GB10 I_{NaL} levels were very similar to ORD11, but in TT06 the current was ~3-fold bigger. **E**. The integrated current density for I_{Ks}, I_{Kr}, I_{CaL} and I_{NaL} for the three original models (grey bars) and the three optimised models (black bars). In the optimised models the current densities for I_{Ks} and I_{Kr} are much more similar to each other than they are in the original models. The changes in current density between the original and optimised models are not as marked for I_{CaL}.

Figure 6

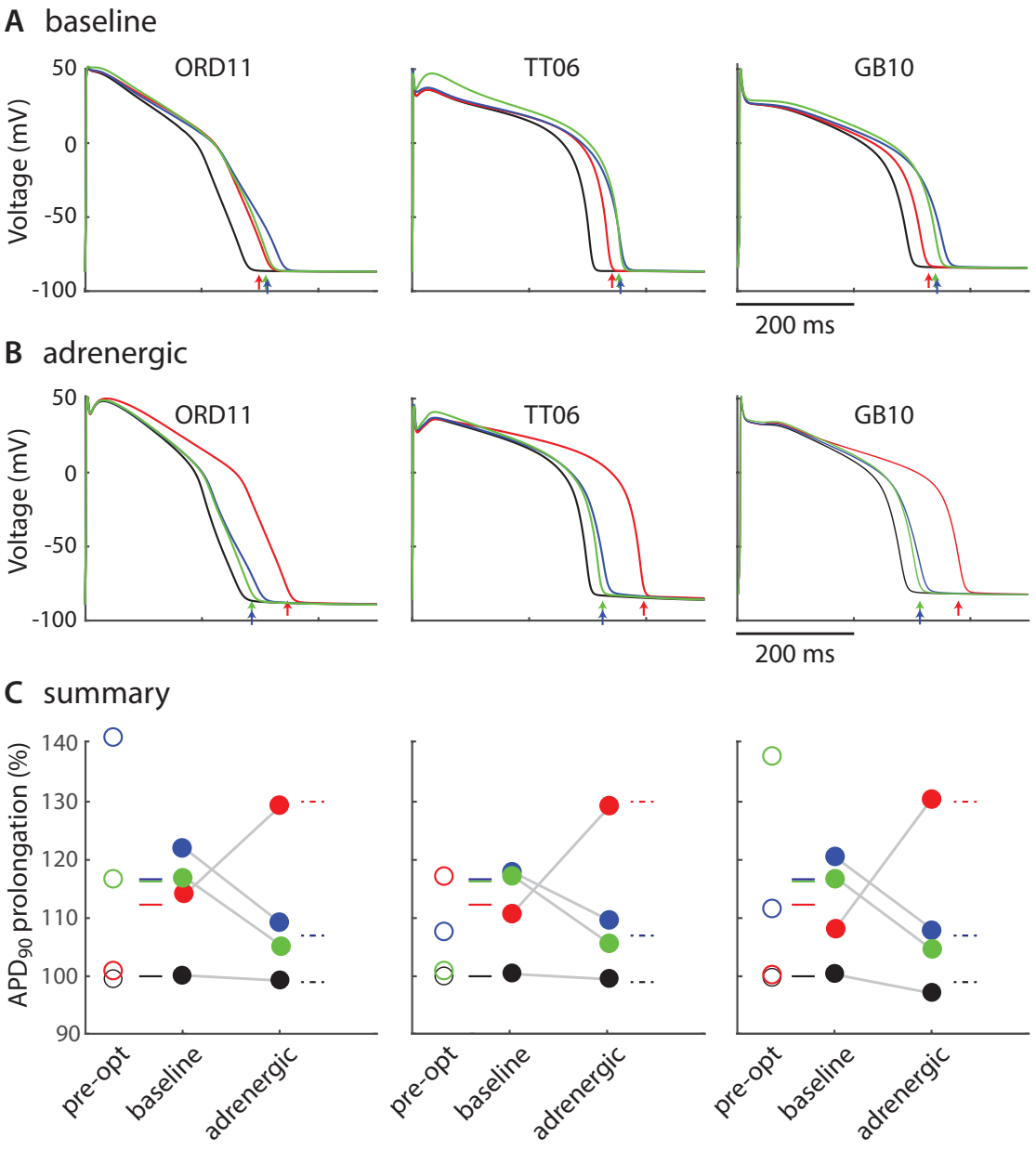

Fig. 6. Action potential waveforms after model optimization.
A) AP waveforms for control (black), LQTS1 (red), LQTS2 (blue) and LQTS3 (green) for the three optimized models. All models show a comparable prolongation for LQTS2 and LQTS3, and a smaller LQTS1 related prolongation. Arrows show the clinically determined levels of QT prolongation that were used as target values. B) AP waveforms of models with adrenergic up-regulation of IKs and ICaL. The prolongation under LQTS1 conditions is the most pronounced in all models after adrenergic stimulation. Arrows again mark the clinically determined prolongation values. C) A summary of the changes in APD90 prolongation in baseline vs. adrenergic shows the same patterns for all three models after the optimization process. The horizontal solid lines show the mean resting QTc values and the dashed horizontal lines show the mean adrenergic QTc values for the clinical data sets. The open circles show the extent of APD90 prolongation in the pre-optimised models and the filled circles show the APD90 prolongation in LQTS1,2,3 under both baseline and adrenergic conditions.

Figure 7

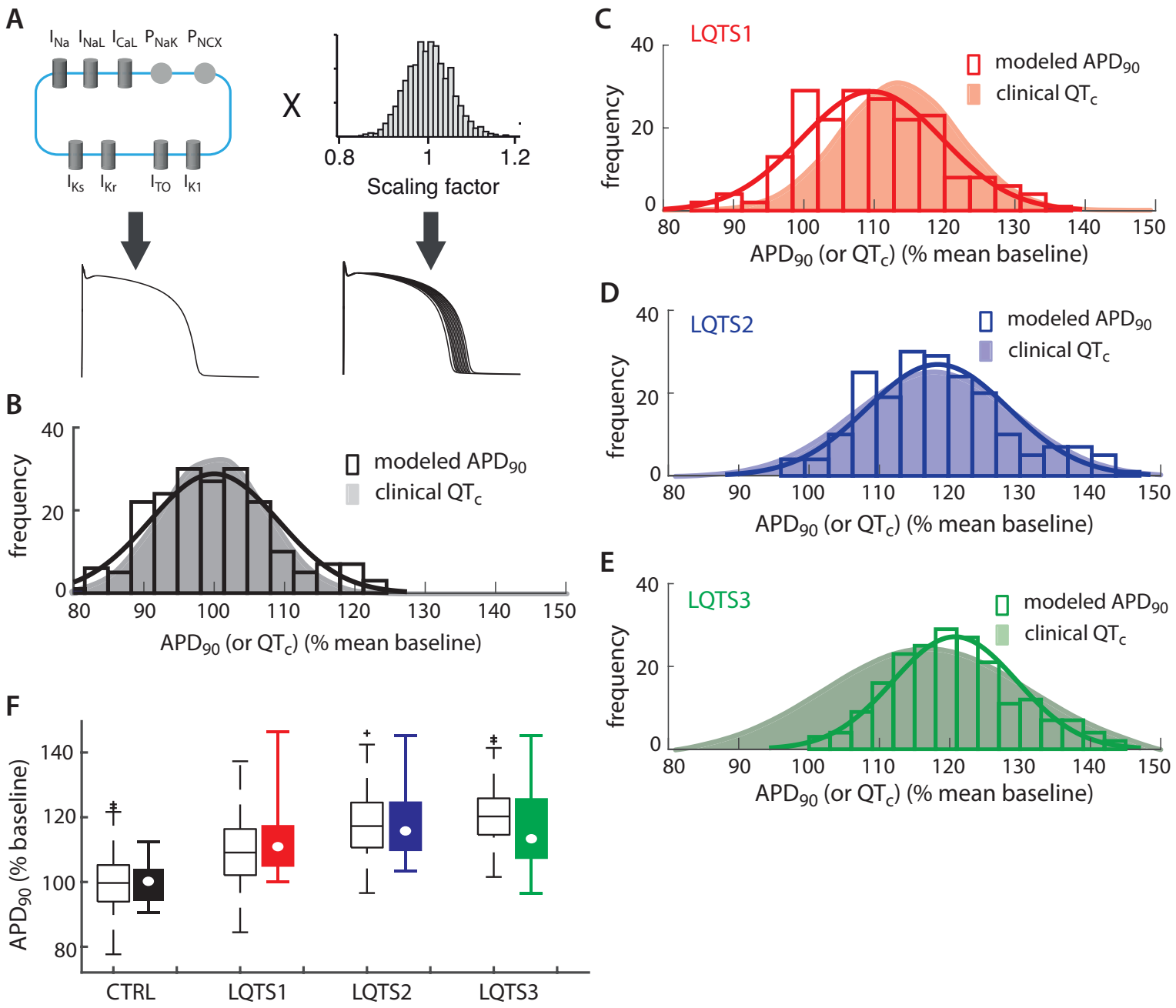

Fig. 7. Simulation of population distribution of QTc values.
A) Simulation pipeline for generation of families of action potentials using the optimized TT06 model as baseline. Ionic conductances in the baseline model are modified using a log–normal distribution of randomised scaling factors and this process is repeated 100 times to generate 100 different APs. The distribution of APD90 values for the 100 APs in B) control, C) LQTS1, D) LQTS2 and E) LQTS3 models shown as a frequency distribution. The solid line shows the best fit Gaussian distribution for the simulated distributions. The shadow shown in grey, red, blue and green show the distributions of the clinical data (taken from Fig. 1). F) A summary of the distributions (shown as box and whisker plots) for the model outputs (open boxes) and the clinical data (closed boxes). Note that the distributions show good similarity between the models and clinical data with the exception of LQTS3 where there is a much larger distribution in the clinical data than that seen in the model outputs.

Supplementary Material

Click here to download Supplementary Material: Supplementary figure 1_rate dependence.eps